Accepted Manuscript

Assessment of fatigue damage evolution in woven composite materials using infra-red techniques

R.K. Fruehmann, J.M. Dulieu-Barton, S. Quinn

PII: S0266-3538(10)00068-0
DOI: 10.1016/j.compscitech.2010.02.009
Reference: CSTE 4638

To appear in: *Composites Science and Technology*

Received Date: 20 August 2009
Revised Date: 30 January 2010
Accepted Date: 7 February 2010

Please cite this article as: Fruehmann, R.K., Dulieu-Barton, J.M., Quinn, S., Assessment of fatigue damage evolution in woven composite materials using infra-red techniques, *Composites Science and Technology* (2010), doi: 10.1016/j.compscitech.2010.02.009

ASSESSMENT OF FATIGUE DAMAGE EVOLUTION IN WOVEN COMPOSITE MATERIALS USING INFRA-RED TECHNIQUES

R.K. Fruehmann, J.M. Dulieu-Barton* and S. Quinn

School of Engineering Sciences, University of Southampton, Southampton, SO17 1BJ, UK

janice@soton.ac.uk*

ABSTRACT

Thermoelastic stress analysis (TSA) is used to study the growth of fatigue damage in single and two ply, 2 x 2 twill woven composite materials. Test specimens were subjected to a uniaxial tensile cyclic loading with maximum stresses of 10, 15 and 20% of the ultimate failure stress. The development of fatigue damage locally within the weft yarns is monitored using high resolution TSA. The specimens were subsequently inspected using optical microscopy to evaluate the location and extent of cracks. Cracks were found in the weft fibres, running transverse to the loading direction. It is demonstrated that the lighter weight fabric is more resilient to damage progression. A signature pattern is identified in the TSA phase data that indicates the onset and presence of fatigue damage in the composite material.

Keywords: A: Textile composites, B: Fatigue, C: Stress concentrations, Thermoelastic stress analysis (TSA)

INTRODUCTION

Fibre-reinforced polymer (FRP) composite materials with textile reinforcements have widespread use in both component manufacture and repair of damaged structures [1]. Their popularity is partially due to ease of handling, ability to drape over complex curvatures, low cost and availability, combined with the typical composite material features of good mechanical performance in terms of the strength and stiffness to weight ratios. Twill woven materials are often used in the surface ply to provide a good surface finish. The use of a textile surface ply, however, provides a challenge for any surface sensing, experimental stress analysis tool due to the heterogeneity of the material surface. The small scale heterogeneity leads to local stress / strain concentrations causing damage evolution, the significance of which is often difficult to assess [2]. Furthermore, where experimental techniques are used in conjunction with FEA, homogenisation of the textile architecture to reduce the cost of numerical simulation means that such small scale effects are typically ignored, making a comparison between measured and calculated data difficult.

The current study investigates the use of thermoelastic stress analysis (TSA) for fatigue assessment in woven FRP composites under tensile loading. TSA is a non-contacting, full-field stress analysis

technique with well documented application to the study of stresses in composite materials [3, 4]. The technique is based on the 'thermoelastic effect' where a small temperature change occurs as result of a change in stress. The temperature change is obtained by means of a sensitive infra-red detector. It has been shown that the thermoelastic response (i.e. the output from the infra-red detector) from an orthotropic material such as a FRP composite is dependent on the orientation of the fibres relative to a set of orthogonal reference axes, which are usually the principal material axes or stress axes [5]. Previous work has been conducted using TSA to study fatigue damage development in laminated non-crimp FRP composites [6]. The work utilised a global approach to damage quantification. However, in composites with woven fibre reinforcements, the weave pattern results in two orthogonal fibre orientations at the surface of the material, with axes that may or may not align with the reference axes. Moreover, because of the interlacing pattern of woven yarns, resin pockets are formed at the weave junctions. As a result the thermoelastic response will vary locally, and even a uniform strain field, as may be expected in simple uniaxial tension, will result in a non-uniform thermoelastic response [7]. However, it is known that even under simple loading conditions, the strains in a woven composite are not uniform [8]. Hence, the interpretation of TSA data from woven composite materials which results from both material and strain variations poses a significant challenge. Therefore, in the current work, both global and local approaches are employed to evaluate the thermoelastic response.

Previous studies on the application of full field strain analysis techniques to woven composites such as digital image correlation or interferometry are few [8-10]. These techniques use quasi-static loading and may require some surface preparation such as the application of a grating or painted speckle pattern. In TSA, measurements can be obtained from a dynamically loaded component in practically real time (less than 5 seconds per measurement) with almost no surface preparation. Data can be collected and analysed in situ, as the material is exposed to fatigue loading.

A cyclic load is required [11] to obtain a TSA measurement. To avoid fatigue damage accumulation during TSA data collection, the necessary applied stresses are maintained at a relatively low level compared to the failure stress of the material. However, a minimum stress amplitude must be achieved in the specimen to affect a measurement. In a typical E-glass / epoxy composite for which, in the fibre direction, a stress change of 1 MPa results in a temperature change of 1.5 mK, the minimum stress threshold is in the range of 10 to 20 MPa, below which stresses cannot be resolved. Experiments involving a 2 x 2 twill woven E-glass / epoxy composite have shown a marked change in the thermoelastic response as individual specimens have been subjected to repeated testing [5]. This indicates that fatigue damage is evolving during the low stress cyclic loading applied to the specimen. This finding has motivated the research described in this paper with a view to identifying the cause of the low stress amplitude, cyclic fatigue damage in textile composites. The purpose of this paper is therefore

to investigate woven composite materials under low amplitude (with a peak stress of less than 20% of the tensile failure stress) cyclic loading conditions. In the literature there are few studies on the effect of low stress amplitude fatigue on woven materials. Ref. [12] is to the authors' knowledge the only work where applied stress levels below 50% of the failure stress are considered. Therefore the aim is both to provide insight into the mechanics of damage evolution in woven polymer composite materials, as well as developing a new understanding of the interpretation of the measured thermoelastic response.

METHODOLOGY

The focus of the work is the onset of fatigue damage and the rate of damage accumulation. Changes in the meso-scale stress field (i.e. at the scale of the yarns) are used to identify and quantify the damage. TSA data was collected at set intervals during the fatigue process. Since TSA relies on dynamic loading, it was possible to obtain the measurements without interruption of the loading cycle. To evolve damage the specimens were fatigued under constant load amplitude. Possible changes in the material stiffness were monitored throughout the fatigue loading by recording changes in the displacement amplitude.

The relationship between the stress changes and the temperature changes that occur as a result of cyclic loading of an orthotropic material can be defined as follows [5]:

$$\Delta T = \frac{-T}{\rho C_p}(\alpha_1 \Delta\sigma_1 + \alpha_2 \Delta\sigma_2) \quad (1)$$

where ΔT is the amplitude of the temperature oscillation, T is the mean surface temperature, ρ is the density, C_p is the specific heat capacity, α_1 and α_2 are the coefficients of thermal expansion (CTE) in the principal material directions and $\Delta\sigma_1$ and $\Delta\sigma_2$ are the amplitudes of the principal stresses.

Equation (1) has been derived for adiabatic conditions, assuming that the elastic temperature change occurs at a sufficiently high rate to ignore any dissipation. In E-glass epoxy composites, due to the low conductivity, this is generally a good assumption [13].

The detector used in this work, a Cedip Silver 480M, is radiometrically calibrated, hence the surface temperature is obtained directly from the system. This enables both the mean surface temperature, T, and the temperature change, ΔT, to be derived from the same infra-red data set. More details regarding the operation of the Cedip system and its application to TSA are given in Ref [7]. During cyclic loading the specimen may heat, particularly in areas of localised damage. Therefore it is useful to eliminate any effects of local surface temperature increase, by normalising the temperature change with the mean surface temperature to give data in the form $\Delta T/T$, which can be considered as a non-dimensional stress metric. As the infra-red detector is an array of 256 x 320 a field of data is obtained and the normalisation is conducted on a pixel-by-pixel basis over the entire field. An added advantage of the normalisation is that variations in laboratory temperature are eliminated and direct comparisons can be made between

different data sets. ΔT is obtained from the temperature data as the magnitude of a fast Fourier transform. To filter out noise in the IR signal, a lock-in amplifier is applied, using the output from the load cell of the test machine as a reference signal. This reference signal also provides a datum that allows a phase angle between the stress change and the thermoelastic response to be obtained. Because of the negative sign in equation (1), a component under tensile loading will have a temperature response that is 180° out of phase with the loading cycle. The phase angle can therefore be used to distinguish between regions undergoing tensile or compressive stress, since in the latter the temperature signal is in phase with the loading cycle. This results in phase angles of either 0° or 180°. Any other value of phase angle indicates departures from a simple linear behaviour, e.g. non-adiabatic behaviour, or viscoelastic heating that may occur at damage sites.

To monitor the damage progression, data was obtained periodically during the fatigue process. Local changes of the material response in all fatigue tests were measured relative to an initial $\Delta T/T$ data set obtained from the undamaged material. To inspect the stress field at the scale of the yarn high resolution optics were employed that provided a spatial resolution of 0.03 mm. The rigid body motion of the specimens exceeded the spatial resolution, so a motion compensation algorithm based on image correlation was applied to the data. This corrected for the lateral displacement of the specimen and allowed clear images to be obtained at the resolution of the yarn.

The specimens were further inspected using an optical microscope before and after fatigue testing to identify, for example, the formation of matrix cracks. Accumulation of fatigue damage identified in the TSA data could thus be correlated to the location and extent of visible damage in the material. Differences in the accumulation and distribution of fatigue damage between different materials could be related to differences in the textile structure and material composition.

MATERIAL SELECTION AND SPECIMEN CONFIGURATION

Two E-glass textiles with a 2 x 2 twill woven roving were selected for this investigation. These were Gurit WRE581T and RE400T with areal densities of 581 and 400 g m^{-2} respectively. The WRE581T textile used 600 tex yarns in both the warp and weft directions, with 5 ends per cm for the warp yarns and 4.6 ends per cm for the weft yarns. The RE400T textile used 336.6 tex yarns with 6.1 ends per cm in the warp direction, and 273.6 tex fibres with 6.6 ends per cm in the weft direction. The E-glass fibres in the WRE581T textile had a diameter of 19 μm while those in the RE400T had a diameter of only 9 μm. The resulting textile dimensions are listed in Table 1. The fibre crimp was measured as the ratio of the out-of-plane deformation to the length of the textile unit-cell.

The textiles were chosen because they represent a weave geometry frequently used to form the surface layer on composite structures. Two textiles were chosen so that the effect of small differences in the weave on the fatigue behaviour could be investigated. To enable an assessment of the effect of the

stacking sequence single and two ply composites were manufactured, one using the WRE581T textile stacked periodically (i.e. the undulations in the warp yarns in adjacent plies were in phase), the other using the RE400T textile stacked symmetrically (i.e. the undulations in the warp yarns in adjacent plies were out of phase).

Table 1: Textile dimensions

Textile	Warp yarn spacing (mm)	Weft yarn spacing (mm)	Warp yarn crimp	Textile thickness (mm)	Fibre volume fraction (%)
WRE581T	2.00	2.17	5 %	0.559	50 %
RE400T	1.65	1.52	4 %	0.405	40 %

The epoxy resin used to form the composite material was Prime 20LV from Gurit, cured using their fast hardener. The composites were manufactured as a flat panel by means of liquid resin infusion, with consolidation at 1 atmosphere of pressure. The specimens were cut from the panel, had end tabs bonded and then were post cured for 16 hours at 50º C.

The specimen dimensions were based around ASTM D 3039. They were nominally 25 mm wide; the gauge length was increased from the standard 150 mm to 250 mm to enable access with the infra-red detector. To eliminate the possibility of slippage that sometimes occurs during long term cyclic loading with standard grips, the specimens were pin loaded *via* 12 mm diameter holes drilled at each end of the specimen. The specimens were fitted with standard 50 mm long end tabs of the same material. Additional 1.5 mm thick aluminium end tabs (40 mm long) were added to serve as a bearing material for the loading pin, eliminating any possible damage growth from the pin-loaded hole.

EXPERIMENTAL ARRANGEMENTS

The fatigue loading conditions were determined from the failure stress of each material. Table 2 shows the failure stress obtained from five quasi-static tensile tests. The specimens were fatigued under constant load amplitude (tension – tension) sinusoidal loading at 10 Hz, using an Instron 8872 servo-hydraulic test machine. The load amplitude was set to cycle from nearly zero giving a minimum stress of between 2 and 6 MPa, to a peak stress of 10, 15 and 20 % of the failure stress for each material. This gives stress ratios greater than 80%. The test was run for 12 hours (440000 cycles) at 10 % of the failure stress and for 5 hours (180000 cycles) at 15 and 20 % of the failure stress. TSA measurements were taken every 600 cycles for the first 4000 cycles and then every 6000 cycles. Each specimen was tested once only. Separate, identical specimens were used for setup and tuning of the servo-hydraulic test machine prior to each test. The displacement amplitude of the actuator was recorded at the start and the end of every test to provide an indication of a change in the global stiffness of the material.

Table 2: Failure stresses of the four materials

Material	WRE581 1 ply	WRE581 2 ply	RE400T 1 ply	RE400 2 ply
Failure Stress (MPa)	416.2	481.5	333.1	340.8
Standard deviation (%)	0.36	4.59	4.29	6.79

Infra-red measurements were obtained using the Cedip system fitted with both a 27 mm standard lens and a G1 high resolution lens. For tests using the 27 mm lens, the detector was positioned with a stand-off distance of approximately 350 mm rotated at an angle of 5 to 10° to the plane of the specimen to avoid a Narcissus effect (i.e. the detector sees its own reflection). This yielded a viewing area of approximately 80 x 100 mm. The G1 lens required a much closer stand-off distance (approximately 8 mm) and a perpendicular orientation of the detector due to the very short focal depth (approximately 0.5 mm) of the G1 optics. The G1 lens covered a viewing area of 8 x 10 mm, roughly one unit cell in the weave pattern.

Post-fatigue examinations were conducted using a macro-scope with x 10 magnification and a microscope up to x 50 magnification. For the microscope examinations, the area studied using TSA was cut out of the specimen, and the cross-section was polished with 4000 grit sandpaper on a polishing wheel.

GLOBAL RESPONSE

The non-dimensional thermoelastic response from all four materials in the undamaged state is shown in Figure 1. The load has been applied in the vertical axis, parallel to the warp fibres. Similarities can be seen in the response from the two single ply specimens and the WRE581T two ply specimen. This diagonal banding in the thermoelastic response is commonly observed in composites made from 2 x 2 twill textiles [7]. The lowest response (blue regions) comes from the warp yarns while the weft yarns are bounded above and below by narrow bands of the highest response (red regions), resulting from the strain concentrations either side of weft yarns as noted in [8]. The RE400T two ply specimen however shows a markedly different pattern. This can be attributed to the difference in the stacking sequence, in-phase periodic for the WRE581T and symmetric for the RE400T. The stacking sequence influences the stress field because it changes how the two plies interact. This may be expected to have an effect on the magnitude of the stress concentrations and hence on the fatigue behaviour of the material. The difference in the magnitude of the response between the different materials is due to the differences in the applied stress range: 41.6 and 48.1 MPa for the WRE581T single and two ply specimens compared with 33.3 and 34.1 MPa for the RE400T single and two ply specimens.

The global change in Young's modulus was obtained by estimating the strain using the change in the displacement amplitude of the actuator and the specimen length between the end tabs (i.e. neglecting the effect of the end tabs on the displacement) and a laminate stress from the applied load and mean specimen cross sectional area. These estimated values for Young's modulus are listed for each specimen in Table 3. At 10% load, the change was negligible in all specimens. At 15 and 20% load, the single ply specimens showed a reduction in stiffness of up to 15%. For the RE400T two ply specimen the changes given in Table 3 are very small and less than the measurement uncertainty. A significant reduction in stiffness for the WRE581T two ply specimen was found only in the 20% loading case. Although the actuator displacement amplitude during a dynamic test does not provide an accurate Young's modulus, these values provide an indication of the reduction in stiffness accompanying the accumulation of damage.

Table 3: Change in global Young's modulus

	RE400T Young's Modulus (GPa)					
	1 ply			2 ply		
Percentage of tensile failure stress	10%	15%	20%	10%	15%	20%
Initial	41.23	38.46	40.16	42.42	44.66	41.85
Final	40.12	34.97	35.07	42.93	44.93	41.04
Percentage reduction	2.69%	9.07%	12.67%	-1.20%	-0.60%	1.94%
	WRE581T Young's Modulus (GPa)					
	1 ply			2 ply		
Percentage of tensile failure stress	10%	15%	20%	10%	15%	20%
Initial	46.04	44.64	42.89	48.68	48.03	48.43
Final	44.01	37.82	36.57		45.84	44.03
Percentage reduction	4.41%	15.28%	14.74%		4.56%	9.09%

The global average of the thermoelastic response was obtained by taking the average of the thermoelastic data from an area, roughly equivalent to that shown in Figure 1, which represents a box of 45 mm in length by 25 mm wide, covering approximately 60 warp and 60 weft cells. The data was then normalised against the response from the undamaged specimen. The global average thermoelastic response is shown in Figure 2, from the virgin material through to the end of the test for the 10, 15 and 20% tensile failure stress cases. (Note that the specimens were not tested to failure.) The two ply RE400T specimen, which shows the lowest level of stress concentrations in the virgin data, also shows the least change in the net thermoelastic response as a result of the fatigue cycling. The single ply

RE400T specimen and the two ply WRE581T specimen display a comparable decrease in the net thermoelastic response. The greatest change is observed in the single ply WRE581T specimen.

Both single ply specimens show a gradual linear decrease in the net thermoelastic response for the 10% loading case. For the two ply specimens the 10% loading case shows no net decrease. For the 15% and 20% loading cases, both single ply specimens show an initial rapid decrease in the net thermoelastic response, followed by a transition to a stable value approximately 20% and 30% lower than the initial data for the RE400T and WRE581T respectively. In contrast, both of the two ply specimens exhibit an approximately linear decrease in the net thermoelastic response for the same two loading cases. This suggests that the interaction between the two plies leads to improved resistance to the accumulation of fatigue damage. Moreover the reduction for the symmetrically stacked laminate shows improved resistance in comparison to the in-phase laminate. The greater resilience of the RE400T compared with the WRE581T and of the two ply specimens compared with the single ply specimens coincides well with the Young's modulus data given in Table 3.

The net decrease in the material response also serves as an indicator relating to the redistribution of stresses in the material. As damage progresses, loads cannot be transferred across cracks, so stresses previously carried by one part of the material are redistributed to other parts of the material. It might therefore be expected that the net global response should remain constant, while the variation in the thermoelastic response across the specimens increases. Figure 2 shows quite clearly that the global response decreases. To estimate the change in the variation in the response the standard deviation in the global response is used. Figure 3 shows the standard deviation in the response, which also decreases proportionally with the average, i.e. the variation in the thermoelastic response remains constant relative to the global average. On closer inspection, it is revealed that the thermoelastic response from the warp cells remains constant throughout the accumulation of fatigue damage, as shown in Figure 4. The decrease in the global thermoelastic response originates solely in the weft yarns, i.e. the yarns orientated transverse to the applied loading direction. This implies firstly, that the damage is occurring in the weft yarns and secondly, that the weft yarns contribute negligibly to the load carrying capacity of the textile in the warp direction.

Figures 5a and 5b show macroscope images from the fatigued specimens of the WRE581T and RE400T single ply specimens after 280000 cycles at the 20% loading case. The specimens were lit from the side, hence revealing subsurface discontinuities in the material. The specimens show some small air bubbles. These are located close to the surface of specimen. It is clear in both images that there are transverse cracks running along the weft yarns. The weave pattern has been overlaid approximately for clarity. It should be noted that the images show a smaller regular pattern originating from the peel ply used in the manufacturing process. This peel ply imprint is on the reverse side of the specimen; all data

was collected from the mould side (i.e. smooth side) of the specimen. Figure 5a shows that cracks in the WRE581T material form as a single crack through the centre of the yarn, in some cases accompanied by smaller parallel cracks along the yarn edges. The cracks grow until they reach a warp yarn, where they stop. The cracks can be seen to continue on the opposite face, interrupted by the crossing warp yarn. In the RE400T material the weft yarns are not as well aligned. The cracks appear more often as two parallel cracks, as shown in Figure 5b. The spacing between the cracks indicates that they occur within the weft yarns, just either side of the yarn centre line. This demonstrates that the damage is evolving locally in the weft yarns and that a global approach as used in [6] is insufficient. It is therefore necessary to examine the behaviour at the yarn level to fully understand the damage accumulation mechanism.

YARN LEVEL STUDY

It is observed in Figure 1 that the thermoelastic response from the weft yarns is approximately 30% greater than that from the warp yarns, while the strongest response originates from the boundary between two weft yarns. This is due to a combination of increased resin content at the yarn interface and the associated increase in the material thermoelastic response, and a strain concentration, as identified in [8]. As the material begins to fatigue the thermoelastic response from the weft yarns decreases. This decrease in response occurs locally, within individual weft yarn undulations. The decrease is found to occur independently in different locations and can happen very early in the fatigue process. In the case of the single ply WRE581T loaded at 20% of the failure stress, the earliest incidence of fatigue damage in a weft yarn was observed after only 200 cycles. The thermoelastic response falls sharply at first, until a point is reached where no further decrease in the thermoelastic response occurs. This continues until the thermoelastic response from all weft yarns has decreased in this way.

To identify in more detail the changes in the thermoelastic response at the weft yarns, data was captured using high resolution optics. Figure 6 shows data from one weft yarn in the single ply WRE581T material, subjected to the 10% loading case, at four different stages in the fatigue process. The data from the virgin material has been subtracted from the corresponding fatigued material data to show the change in the $\Delta T/T$ field. Figure 6a shows that no damage has occurred in the yarn after 34000 cycles. Damage initiates at approximately 40000 cycles in the centre of the yarn. This is identified by the decrease in the signal (blue) at the centre of the yarn, and the two small regions of increased response (red) either side. By 46000 cycles the damage has reached the warp yarns on either side and the damage evolution is arrested. The normalised thermoelastic response from the whole region of the weft yarn decreases by approximately 2×10^{-4} (approximately 30% of the original value). No further decrease in the signal occurs; neither does the affected area grow. The two small regions of increased response at the lateral edges of the weft yarn remain, but do not develop further.

The decrease in the thermoelastic response can be linked to a decoupling of the weft yarn from the global strain field as a result of a transverse crack in the centre, or along the edges. The two small regions either side of the yarn centre resemble crack tip stresses found in metals [14] supporting the idea that the change in the thermoelastic response is due to changes in the stress field around a growing crack. At either end of the crack, the material is bounded by the warp yarns which are able to bridge the crack, explaining why the damage stops growing when it reaches this point. Corresponding data from the centre of a warp yarn shows no measurable change in the thermoelastic response. This data thereby adds detail and confirms the findings from the global TSA data and the macroscope images; however, it does not provide any additional information regarding the mechanics that lead to the damage, or the source of the thermoelastic response. Also, the subtractive method for establishing the presence or severity of damage as shown above assumes *a priori* knowledge of a virgin, undamaged state. It is desirable to establish a means of identifying damage without the virgin data set for comparison.

DAMAGE IDENTIFICATION

The cross-section parallel to the warp yarns was examined under a microscope, up to a magnification of x 50; micrographs are shown in Figure 7. In the WRE581T material, the cracks can be seen to penetrate the full thickness of the weft yarn. Upon reaching the warp yarns, the cracks change direction to follow the edge of the warp yarns, resulting in a delamination between the warp and weft yarns. This coincides with findings by Osada and Nakai. [12]. An example is shown in Figure 7a, taken from the WRE581T single ply specimen after 180000 cycles at 20% of the failure stress. The crack is highlighted by a thin black line. The cracks in the RE400T material were much finer (see Figure 7b), and through yarn cracks could not be identified in any of the specimens. Only a shallow penetration of 40 to 110 μm could reliably be measured as shown in Figure 7b. The difference in the size of the cracks between the WRE581T and the RE400T materials might be due to the difference in the fibre diameter between the two materials. The images do however imply that fatigue is more acute in the heavier textile, with greater yarn crimp and larger fibre diameter.

The delamination between the warp and weft yarns, shown in Figure 7a, results from the shear forces between the two yarns. The delamination allows the weft yarns to slide transversely and accommodate increased crimp as the warp yarns straighten under the load. It was observed that surface undulations and edge waviness were most pronounced in the specimens with the greatest damage, indicating that straightening of the warp yarns results in a transverse contraction of the weft yarns. This mechanism will result in a shear strains at the interface between the warp and weft yarns leading to viscoelastic heating in regions of large strain. Furthermore frictional heating after the delamination will lead to heat generation. These nonlinear effects can be expected to show in the phase data which is investigated next.

Figure 8 shows the thermoelastic phase data for the same region shown in Figure 6, but including also the adjacent yarns. The pattern of the weave has been superimposed on the data in black. It is immediately striking that there is a phase difference between the warp and the weft yarns in the undamaged state, measured as 8º. The response from the weft yarns is initially 180° out of phase with the load while that of the warp yarns is 188° out of phase. This difference in the phase angle could be due to a through yarn stress gradient, resulting from the yarn crimp, which imposes a bending stress on the yarns additional to the net tensile stress carried. The crimp also induces through a thickness compressive stress which decays towards the surface of the yarn. The same is true for the transverse yarns, except that the direction of the yarn bending is opposite to that in the warp yarns. Therefore to explain the phase shift in the undamaged state, the full three-dimensional stress field must be considered. Of interest in the context of damage assessment, it can be seen that as the damage initiates, the phase angle in the weft yarn increases to 190° in the centre, while the two small stress concentrations either side display a decrease of approximately 10° in the phase angle. A line plot through the centre of the weft yarn shows the profile of the phase along the length of the weft yarn, see Figure 9. (The weft yarn lies between 2 and 6 mm along the x-axis.) Once the damage has fully developed, there is a 20° phase shift between the central region and the ends of the crack. This pattern propagates in exactly the same way as the thermoelastic response shown in Figure 6, thereby providing a signature pattern in the phase data that allows fatigue damage to be identified, without the requirement for a data set of the undamaged material.

DISCUSSION

A change in the Young's modulus, i.e. residual stiffness, has in the past often been used as a measure of fatigue damage [15]. However, this change can be gradual, and it is not readily applicable to full scale assessments, neither does it provide information on the nature of the damage accumulation. The current work demonstrates how TSA can be used to identify damage in a heterogeneous material, such as a woven FRP composite. The strength of the technique lies in the ability to obtain data-rich measurements directly from the dynamically loaded component without interruption to the damaging process. The straight forward temperature measurement can indicate viscoelastic heating often associated with damage. Averaging over many measurements and load cycles enables very small temperature anomalies to be identified, of the order of a few mK. For the low stress fatigue cycling used in this work a simple map of temperature evolutions (shown in Figures 10a and b) shows that viscoelastic heating is not occurring and that standard themographic inspections would not identify the damage.

Figures 11a and b show the thermoelastic ΔT field; once again, the damage is not apparent. The damage becomes clear when a direct comparison with the virgin data can be made, as shown in Figures 12a and b. Here the non-dimensional form ($\Delta T/T$) is subtracted from undamaged data set to enable the damage site to be located precisely, and clearly indicates that the damage mechanism is the formation of

matrix cracks in the weft yarns. The work in the paper shows that the damage mechanism is the same for two materials with different damage resilience and different fibres, but similar weave geometries.

Since in an industrial situation the undamaged $\Delta T/T$ field may not be known, the identification of a signature pattern in the thermoelastic phase data as shown in Figures 13a and b is an important outcome. A phase difference between the warp and weft yarns that may be due to either heat transfer between the two, or a mechanical effect resulting in asynchronous loading of the two sets of yarns is observed. Viscoelastic heating is considered an unlikely explanation for this phase shift since localised heating is not observed in the thermal data (i.e. Figures 10a and b). The variation in the phase data does not impair the ability to detect damage. A change in the phase angle at the damage site produces an easily identifiable signature pattern, similar to that found in the subtracted $\Delta T/T$ data. Thus the phase data can be used to identify damage in the absence of *a priori* knowledge of the virgin thermoelastic field.

CONCLUSIONS

The study highlights the potential for fatigue damage to accumulate rapidly in woven composite materials, even at low stress levels. The damage accumulation is most pronounced in single ply composites such as may be used as the face sheet material in sandwich structures. It is shown that small differences in the textile, for example the use of a different yarn, can result in greatly improved resistance to damage initiation. Also, the interaction between plies within a laminate can substantially reduce the susceptibility to the development of this type of fatigue. This has implications for applications in which heavier weight textiles and reduced ply numbers are used to reduce manufacturing costs, or where sandwich structures with very thin face sheets are used to reduce weight. Further studies are required to identify if the textile weight, the yarn crimp or the fibre diameter is the most critical parameter influencing the susceptibility to this type of damage accumulation. While the development of matrix cracks does not lead directly to failure at the load levels used in the tests, it should be noted that the presence of cracks at the surface may lead to greater susceptibility towards environmental degradation, such as the ingress of water.

The potential to identify the growth of small scale damage by means of TSA has been clearly demonstrated. By considering the thermoelastic response in a non-dimensional form, data obtained under different conditions (i.e. collected at different ambient temperatures) can be reliably compared. TSA thereby provides a robust tool for evaluating damage development in structural FRP composite components.

The interpretation of a signature pattern for a particular type of defect can be of great use in practical engineering applications. The use of the phase data to identify damage enables the technique to be applied without *a priori* knowledge of the material thermoelastic response in a virgin state. The phase data also shows potential to provide new insight into the meso-scale mechanics of woven materials. The

deeper implications of small phase shifts in the undamaged state between the warp and weft yarns require further investigation. It is proposed that the phase change is due to heat transfer resulting from stress gradients in the through thickness direction.

The study has demonstrated the successful identification of micro-cracking in woven composite materials using TSA. An improved understanding of the thermoelastic response from this type of material has been achieved enabling greater confidence in the interpretation of TSA data from woven composite materials. Fatigue in woven composites at low loading levels has been observed together with the signature pattern enabling the damage to be identified. Therefore the study represents significant progress in the application of TSA in the study of the behaviour of woven composite materials.

ACKNOWLEDGEMENTS

The authors are grateful for the support of the UK Engineering and Physical Sciences Research Council and Airbus UK.

REFERENCES

[1] Xue P., Peng X., Cao J. A non-orthogonal constitutive model for characterizing woven composites. Composites: Part A 2003;34:183–193.

[2] Carvalho N. V., Pinho, S. T., Robinson P. Compressive failure of 2D woven composites. Proceedings of the 17th International Conference on Composite Materials, Edinburgh, UK: IOM Communications Ltd. 2009. on CD.

[3] Dulieu-Barton J M, Stanley P. Development and applications of thermoelastic stress analysis. Journal of Strain Analysis 1998;33:93-104.

[4] Pitarresi G, Patterson E A. A review of the general theory of thermoelastic stress analysis. Journal of Strain Analysis 2003;38:405-417.

[5] Stanley P, Chan W K. The application of thermoelastic stress analysis techniques to composite materials. Journal of Strain Analysis 1988;23:137-143.

[6] Emery T R, Dulieu-Barton J M. Thermoelastic stress analysis of damage mechanisms in composite materials. Composites A, *in press*.

[7] Fruehmann R K, Dulieu-Barton J M, Quinn S. On the thermoelastic response of woven composite materials. Journal of Strain Analysis 2008;43:435-450.

[8] Lee J, Molimard J, Vautrin A, Surrel Y. Digital phase-shifting grating shearography for experimental analysis of fabric composites under tension. Composites - Part A: Applied Science and Manufacturing 2004;35:849-859.

[9] Ivanov D, Ivanov S, Lomov S, Verpoest I. Strain mapping analysis of textile composites. Optics and Lasers in Engineering 2009;47:360-370.

[10] Hale R D. An experimental investigation into strain distribution in 2D and 3D textile composites. Composite Science and Technology 2003;63:2171-2185.

[11] Boyce B R. TSA signal processing and data collection. In: Harwood N, Cummings W M, editors. Thermoelastic Stress Analysis. Bristol: IOP Publishing Ltd, 1991.

[12] Osada T, Nakai A, Hamada H. Initial fracture behavior of satin woven fabric composites. Composite Structures 2003;61:333-339.

[13] Wong A K. A non-adiabatic thermoelastic theory for composite laminates. Journal of Physics and Chemistry of Solids 1991;52:483-494.

[14] Dulieu-Barton J M, Fulton M C, Stanley P. The analysis of thermoelastic isopachic data from crack tip stress fields. Fatigue and Fracture of Engineering Materials and Structures 2000;23:301-313

[15] Mayer R M. Fatigue considerations. In: Mayer R M, editor. Design of composite structures against fatigue: applications to wind turbine blades. Bury St. Edmunds: Mechanical Engineering Publications Ltd., 1996.

FIGURES

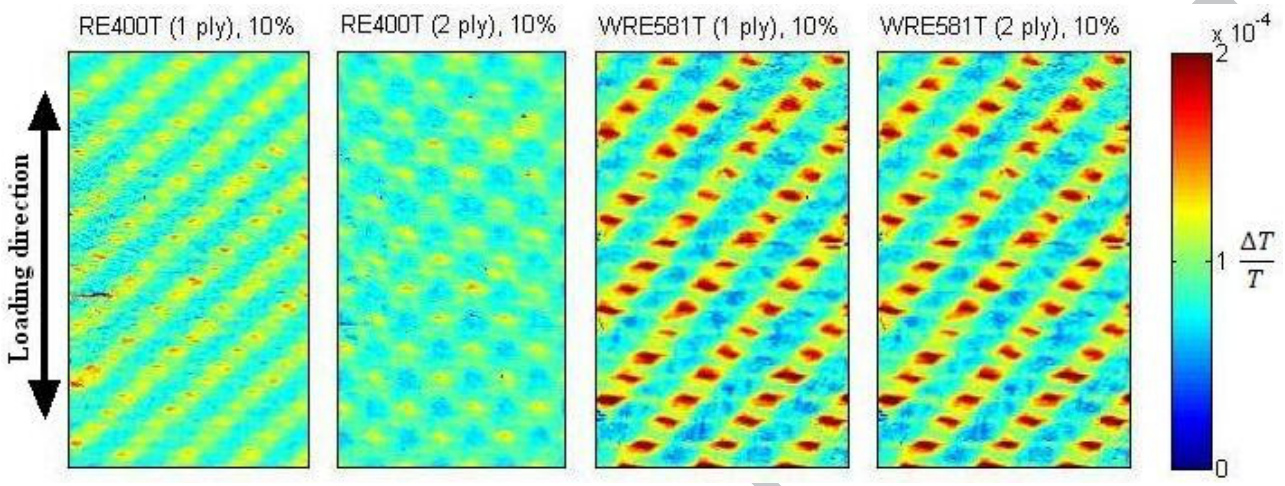

Figure 1: Measured non-dimensional $\Delta T/T$ field from virgin materials (200 cycles) where the peak of the cycle is at 10% of the tensile failure stress

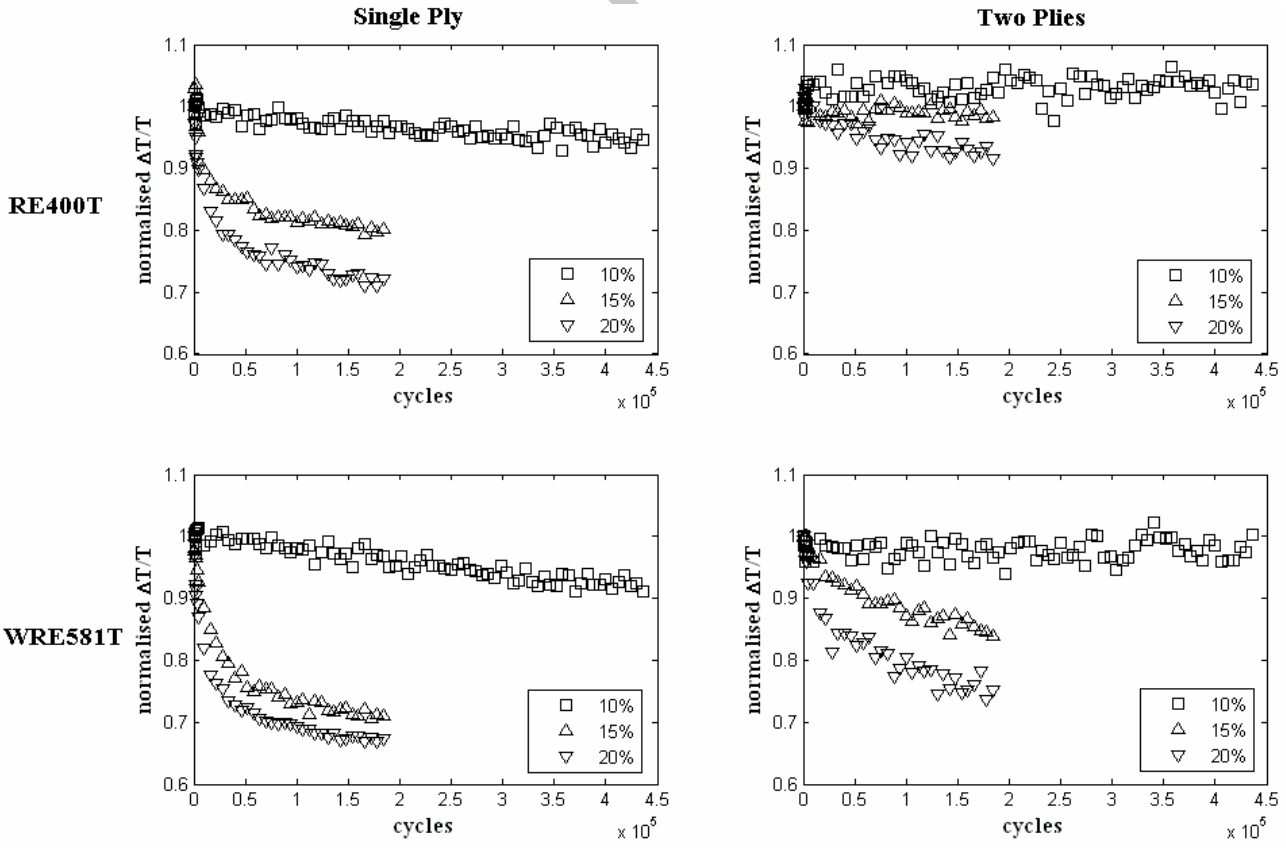

Figure 2: Global averaged $\Delta T/T$ (in the legend 10%, 15% and 20% refers to the percentage of tensile failure stress)

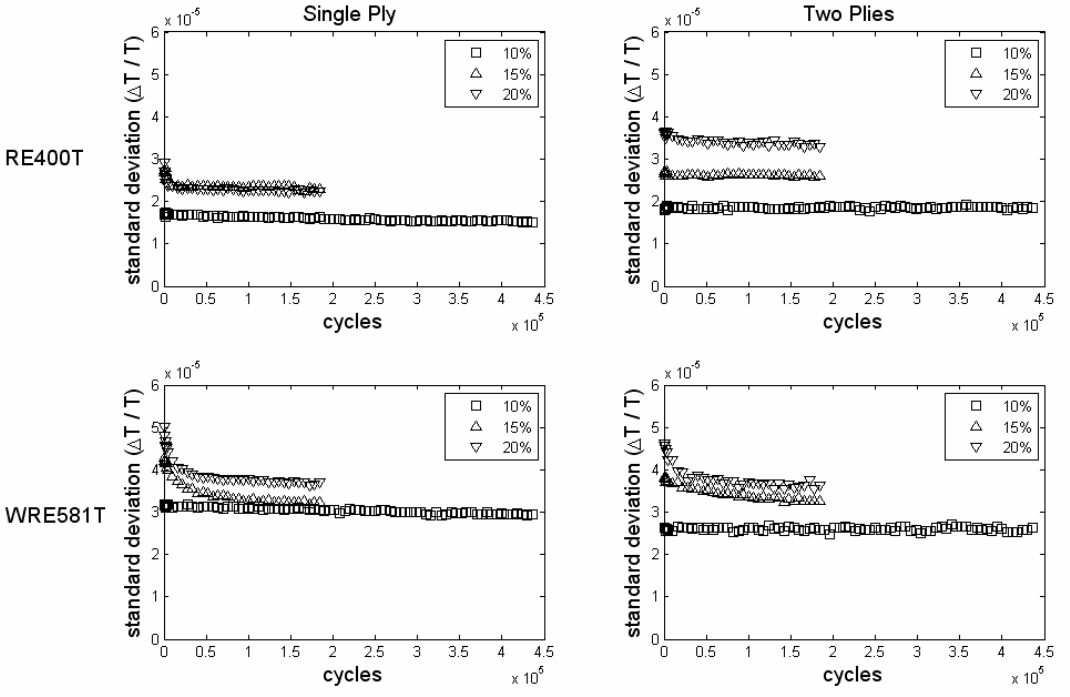

Figure 3: Standard deviation of globally averaged $\Delta T/T$ (in the legend 10%, 15% and 20% refers to the percentage of tensile failure stress)

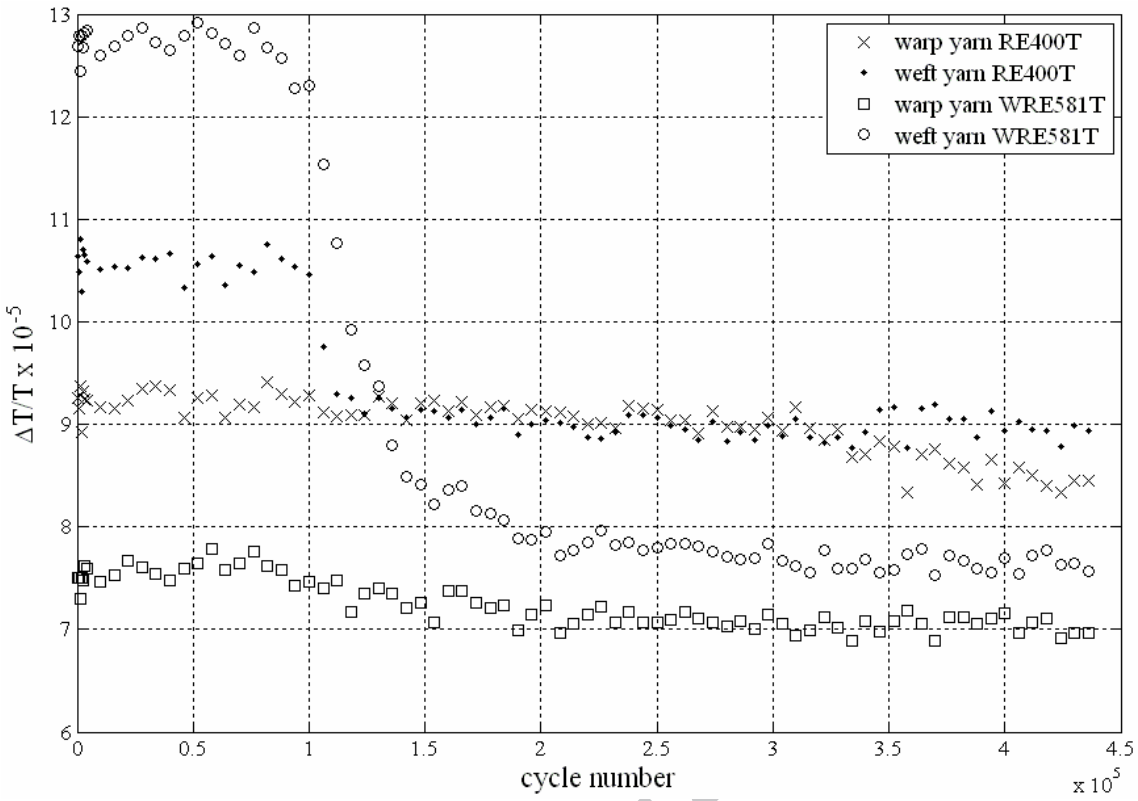

Figure 4: Local non-dimensional $\Delta T/T$ from a typical warp and weft yarn in both the RE400T and WRE581T single ply composites, loaded at 10% of the failure load.

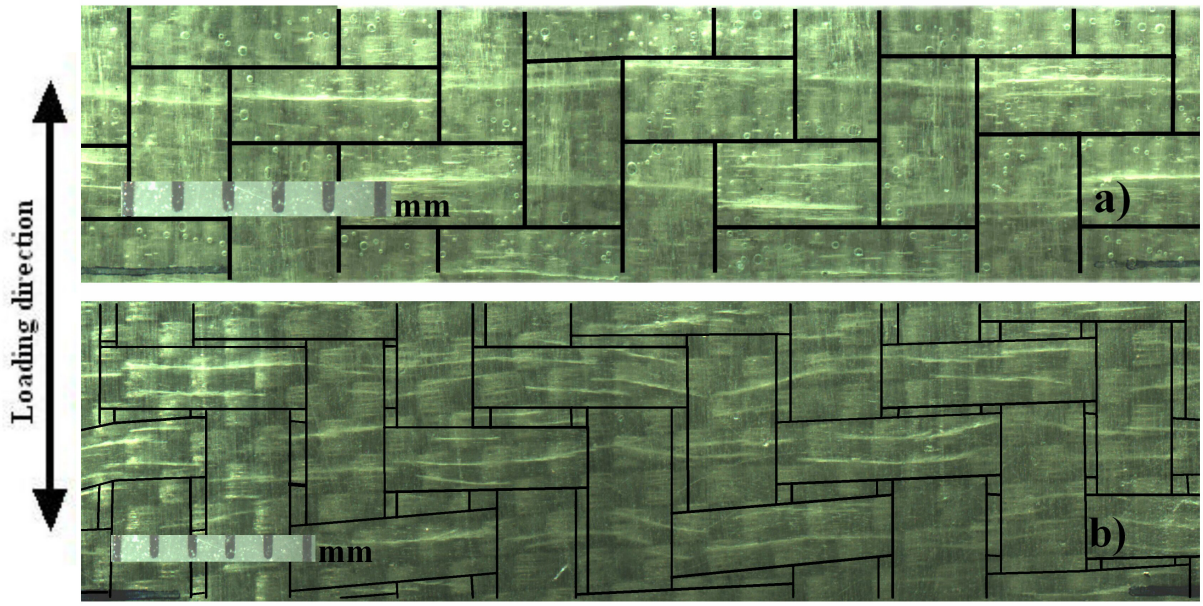

Figure 5: Macroscope images from WRE581T a) single ply, b) two ply specimens after 184000 cycles

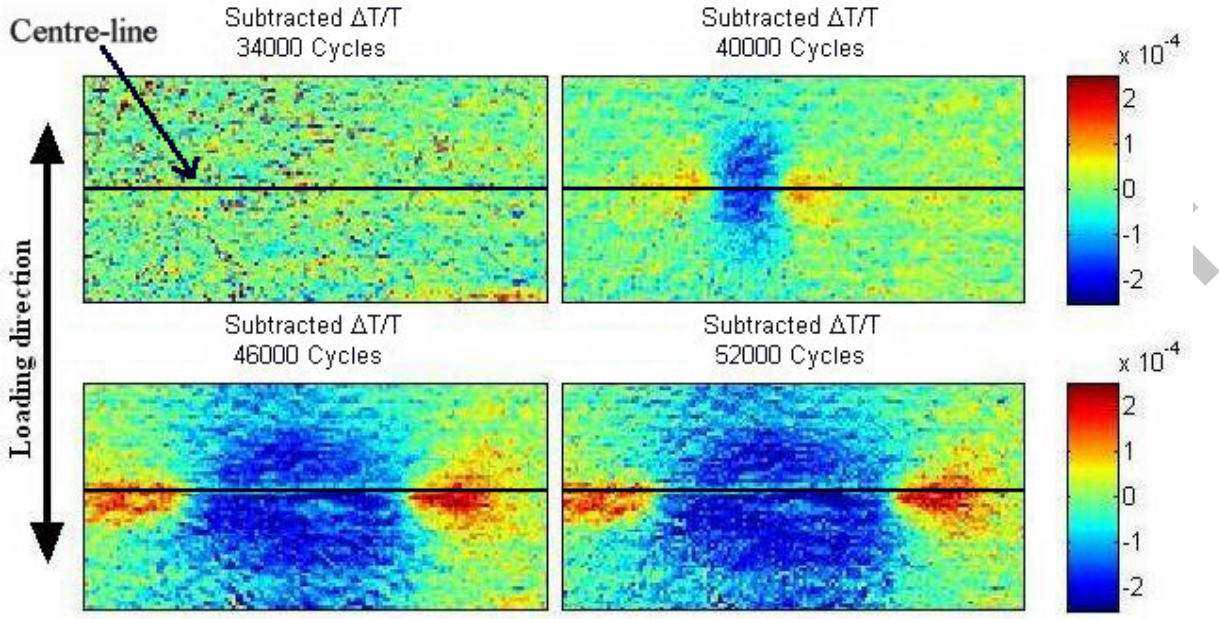

Figure 6: Subtracted Δ*T*/*T* image of a single weft cell of the single ply, WRE581T specimen loaded at 10 % of the failure stress

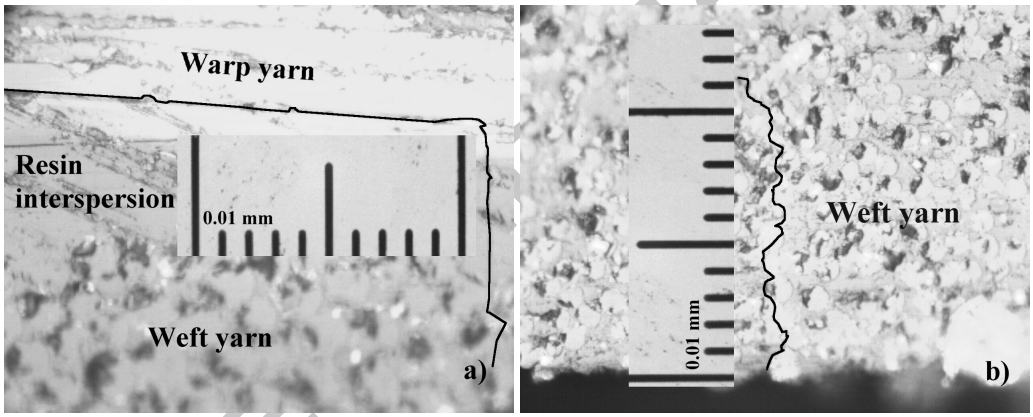

Figure 7: x 50 magnification images of the cracks in the weft yarns with 10 µm graticule a) WRE581T warp / weft interface crack propagation, b) RE400T weft surface crack

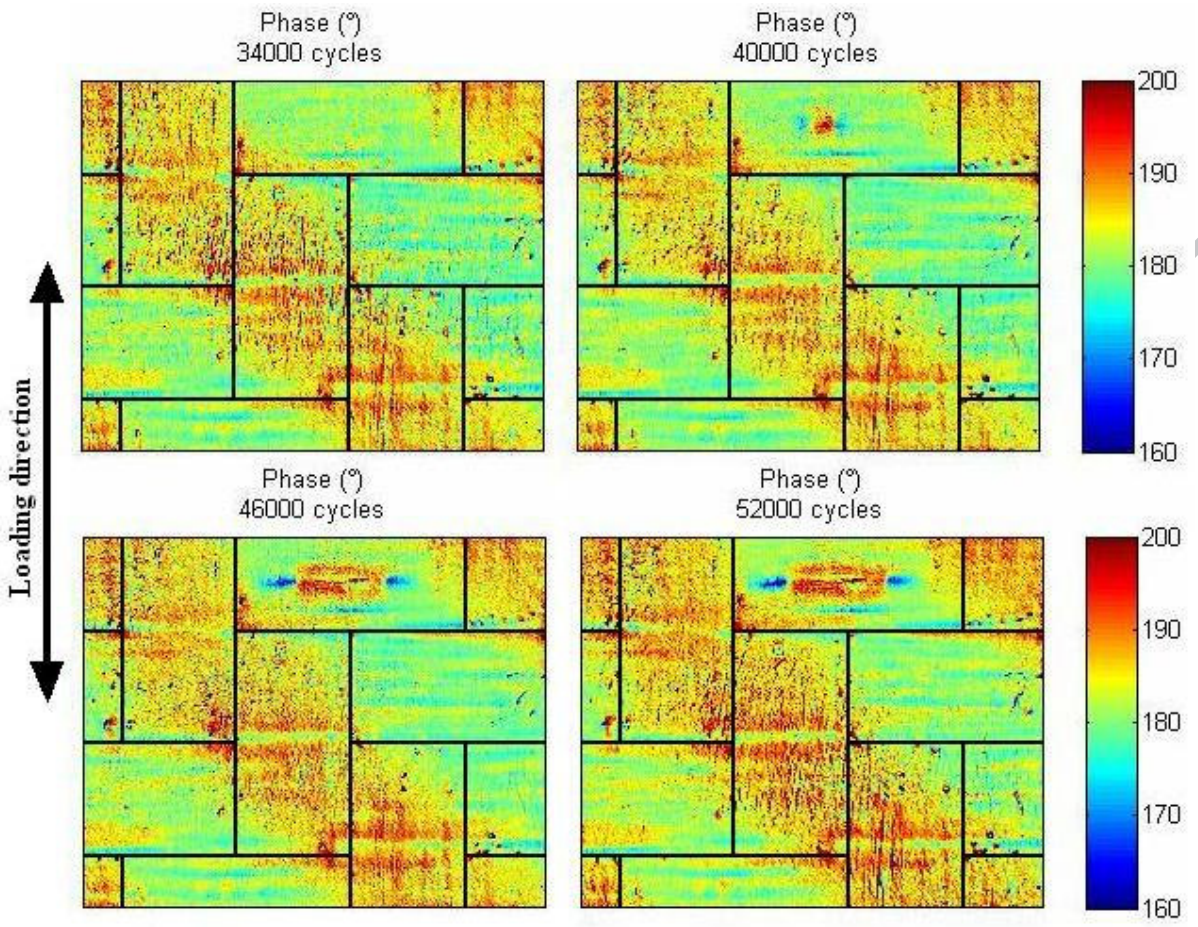

Figure 8: Phase data from the single ply, WRE581T specimen loaded at 10 % of the failure stress

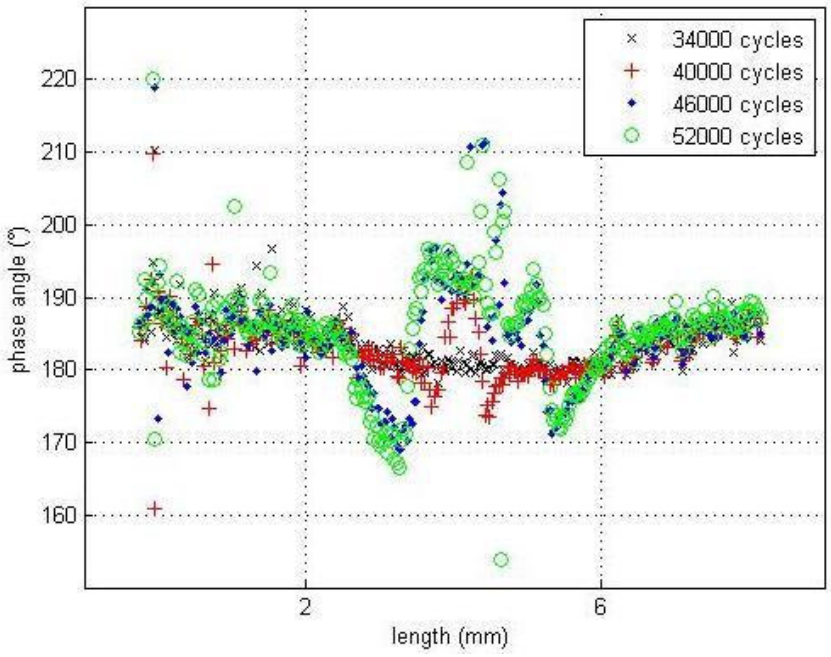

Figure 9: Line plot along the centreline of the weft cell shown in Figure 6 for increasing damage states.

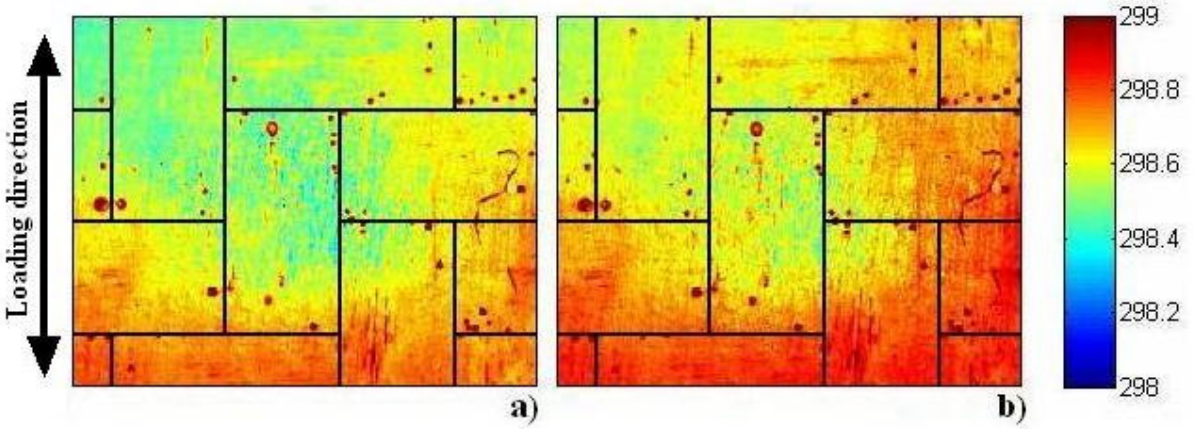

Figure 10: Mean surface temperature images from the WRE581T single ply material, under 10% loading after a) 40000 cycles and b) 46000 cycles.

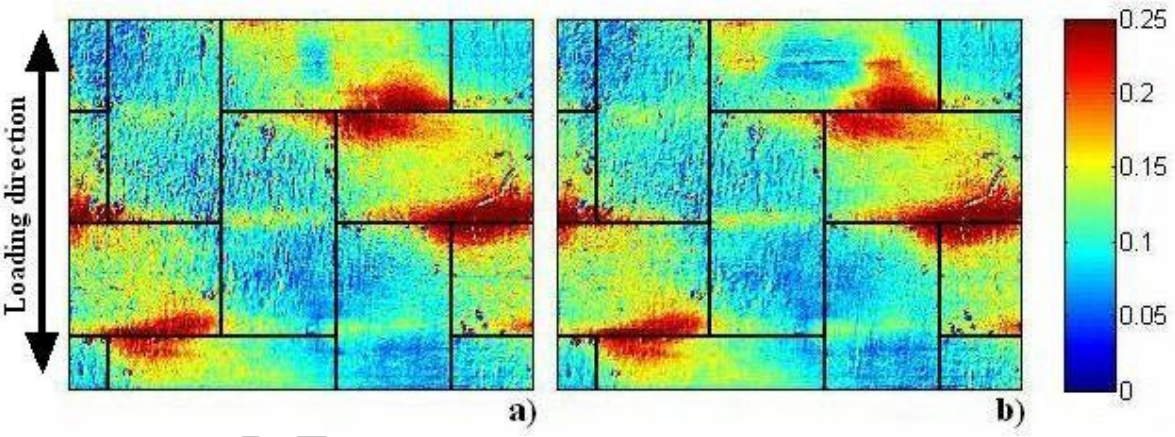

Figure 11: ΔT images from the WRE581T single ply material, under 10% loading after a) 40000 cycles and b) 46000 cycles.

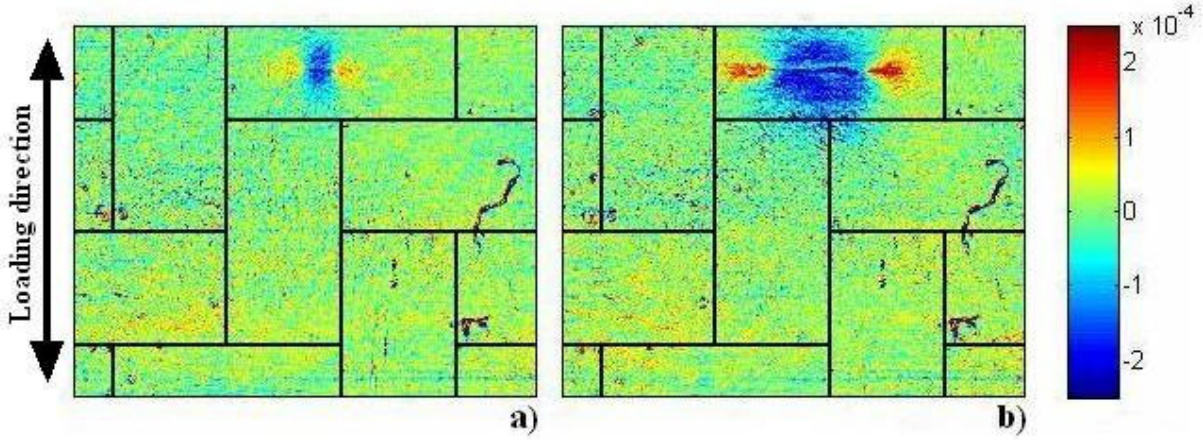

Figure 12: Subtracted $\Delta T/T$ images from the WRE581T single ply material, under 10% loading after a) 40000 cycles and b) 46000 cycles.

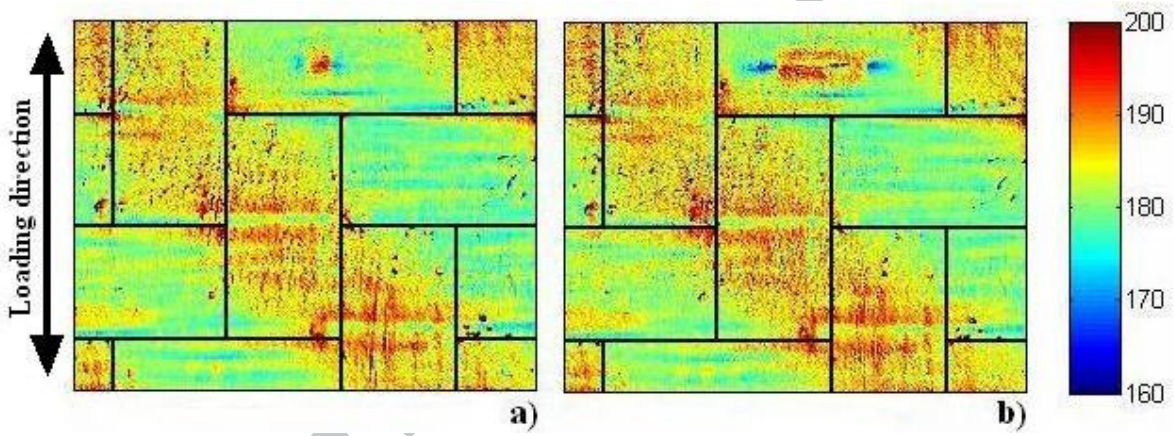

Figure 13: Phase data from the WRE581T single ply material, under 10% loading after a) 40000 cycles and b) 46000 cycles.